Research Article | Vol. 25, No. 7 | 3 Apr 2017 | OPTICS EXPRESS 7984

Optics EXPRESS

Submillisecond-response liquid crystal for high-resolution virtual reality displays

FANGWANG GOU,[1] HAIWEI CHEN,[1] MING-CHUN LI,[2] SEOK-LYUL LEE,[2] AND SHIN-TSON WU[1,*]

[1]College of Optics and Photonics, University of Central Florida, Orlando, Florida 32816, USA
[2]AU Optronics Corp., Hsinchu Science Park, Hsinchu 300, Taiwan
[*]swu@ucf.edu

Abstract: We report a vertically-aligned liquid crystal display (LCD) device with submillisecond response time, high transmittance, and low operation voltage. The top substrate has a common electrode, while the bottom substrate consists of hole-patterned fringing-field-switching (FFS) pixel electrodes. A negative dielectric anisotropy LC is employed. In the voltage-on state, the LC directors are reoriented by the fringing fields surrounding the hole area and by the longitudinal and fringe fields outside the hole area. After design optimization, we are able to achieve 85% peak transmittance under crossed circular polarizers. During the relaxation process, the standing walls exert a strong restoring force, leading to submillisecond gray-to-gray response time. Moreover, this device enables high resolution density because only one thin-film transistor per pixel is needed and the bottom FFS electrode has built-in capacitor. This device is particularly attractive for the emerging virtual reality displays.

© 2017 Optical Society of America

OCIS codes: (160.3710) Liquid crystals; (230.3720) Liquid-crystal devices; (120.2040) Displays.

References and links

1. O. Cakmakci and J. Rolland, "Head-worn displays: a review," J. Disp. Technol. **2**(3), 199–216 (2006).
2. H. G. Hoffman, W. J. Meyer 3rd, M. Ramirez, L. Roberts, E. J. Seibel, B. Atzori, S. R. Sharar, and D. R. Patterson, "Feasibility of articulated arm mounted Oculus Rift Virtual Reality goggles for adjunctive pain control during occupational therapy in pediatric burn patients," Cyberpsychol. Behav. Soc. Netw. **17**(6), 397–401 (2014).
3. H. Kikuchi, M. Yokota, Y. Hisakado, H. Yang, and T. Kajiyama, "Polymer-stabilized liquid crystal blue phases," Nat. Mater. **1**(1), 64–68 (2002).
4. Y. Huang, H. Chen, G. Tan, H. Tobata, S.-I. Yamamoto, E. Okabe, Y. F. Lan, C. Y. Tsai, and S. T. Wu, "Optimized blue-phase liquid crystal for field-sequential-color displays," Opt. Mater. Express **7**(2), 641–650 (2017).
5. J. S. Patel and R. B. Meyer, "Flexoelectric electro-optics of a cholesteric liquid crystal," Phys. Rev. Lett. **58**(15), 1538–1540 (1987).
6. A. Varanytsia and L. C. Chien, "Bimesogen-enhanced flexoelectro-optic behavior of polymer stabilized cholesteric liquid crystal," J. Appl. Phys. **119**(1), 014502 (2016).
7. F. Castles, S. M. Morris, D. J. Gardiner, Q. M. Malik, and H. J. Coles, "Ultra-fast-switching flexoelectric liquid-crystal display with high contrast," J. Soc. Inf. Disp. **18**(2), 128–133 (2010).
8. H. Chen, F. Gou, and S. T. Wu, "A submillisecond-response nematic liquid crystal for augmented reality displays," Opt. Mater. Express **7**(1), 195–201 (2017).
9. D. J. Channin, "Triode optical gate: A new liquid crystal electro-optic device," Appl. Phys. Lett. **26**(11), 603–605 (1975).
10. T. H. Choi, Y. J. Park, J. W. Kim, and T. H. Yoon, "Fast grey-to-grey switching of a homogeneously aligned liquid crystal device," Liq. Cryst. **42**(4), 492–496 (2015).
11. Y. Iwata, M. Murata, K. Tanaka, A. Jinda, T. Ohtake, T. Shinomiya, and H. Yoshida, "Novel super-fast-response, ultra-wide temperature range VA-LCD," SID Int. Symp. Digest Tech. Papers **44**(1), 431–434 (2013).
12. Y. Chen, F. Peng, T. Yamaguchi, X. Song, and S. T. Wu, "High performance negative dielectric anisotropy liquid crystals for display applications," Crystals **3**(3), 483–503 (2013).
13. S.-T. Wu, U. Efron, and L. D. Hess, "Birefringence measurements of liquid crystals," Appl. Opt. **23**(21), 3911–3915 (1984).
14. I. Haller, "Thermodynamic and static properties of liquid crystals," Prog. Solid State Chem. **10**, 103–118 (1975).
15. S.-T. Wu, "Birefringence dispersions of liquid crystals," Phys. Rev. A Gen. Phys. **33**(2), 1270–1274 (1986).

#286586 https://doi.org/10.1364/OE.25.007984
Journal © 2017 Received 10 Feb 2017; revised 21 Mar 2017; accepted 21 Mar 2017; published 28 Mar 2017

Optics EXPRESS

16. S.-T. Wu and C. S. Wu, "Rotational viscosity of nematic liquid crystals A critical examination of existing models," Liq. Cryst. **8**(2), 171–182 (1990).
17. H. Chen, M. Hu, F. Peng, J. Li, Z. An, and S. T. Wu, "Ultra-low viscosity liquid crystals," Opt. Mater. Express **5**(3), 655–660 (2015).
18. S. H. Lee, S. L. Lee, and H. Y. Kim, "Electro-optic characteristics and switching principle of a nematic liquid crystal cell controlled by fringe-field switching," Appl. Phys. Lett. **73**(20), 2881–2883 (1998).
19. K. H. Kim, K. H. Lee, S. B. Park, J. K. Song, S. N. Kim, and J. H. Souk, "Domain divided vertical alignment mode with optimized fringe field effect," Proc. Asia Display **98**, 383–386 (1998).
20. T.-H. Choi, S.-W. Oh, Y.-J. Park, Y. Choi, and T.-H. Yoon, "Fast fringe-field switching of a liquid crystal cell by two-dimensional confinement with virtual walls," Sci. Rep. **6**(1), 27936 (2016).
21. H. Chen, G. Tan, Y. Huang, Y. Weng, T. H. Choi, T. H. Yoon, and S. T. Wu, "A low voltage liquid crystal phase grating with switchable diffraction angles," Sci. Rep. **7**, 39923 (2017).
22. A. Lien, "Extended Jones matrix representation for the twisted nematic liquid crystal display at oblique incidence," Appl. Phys. Lett. **57**(26), 2767–2769 (1990).
23. H. Chen, Y. Gao, and S. T. Wu, "n-FFS vs. p-FFS: Who wins?" SID Int. Symp. Digest Tech. Papers **46**(1), 735–738 (2015).
24. S. H. Lee, H. Y. Kim, I. C. Park, B. G. Rho, J. S. Park, H. S. Park, and C. H. Lee, "Rubbing-free, vertically aligned nematic liquid crystal display controlled by in-plane field," Appl. Phys. Lett. **71**(19), 2851–2853 (1997).
25. H. Yoshida, Y. Nakanishi, T. Sasabayashi, Y. Tasaka, and K. Okamoto, "Fast-switching LCD with multi-domain vertical alignment driven by an oblique electric field," SID Int. Symp. Digest Tech. Papers **31**(1), 334–337 (2000).
26. J. W. Park, Y. J. Ahn, J. H. Jung, S. H. Lee, R. Lu, H. Y. Kim, and S. T. Wu, "Liquid crystal display using combined fringe and in-plane electric fields," Appl. Phys. Lett. **93**(8), 081103 (2008).
27. S. T. Wu, "Nematic liquid crystal modulator with response time less than 100 μs at room temperature," Appl. Phys. Lett. **57**(10), 986–988 (1990).
28. T. Kurita, "Moving picture quality improvement for hold-type AM-LCDs," SID Int. Symp. Digest Tech. Papers **32**(1), 986–989 (2001).
29. Y. Igarashi, T. Yamamoto, Y. Tanaka, J. Someya, Y. Nakakura, M. Yamakawa, S. Hasegawa, Y. Nishida, and T. Kurita, "Summary of moving picture response time (MPRT) and futures," SID Int. Symp. Digest Tech. Papers **35**(1), 1262–1265 (2004).
30. F. Peng, H. Chen, F. Gou, Y.-H. Lee, M. Wand, M.-C. Li, S.-L. Lee, and S.-T. Wu, "Analytical equation for the motion picture response time of display devices," J. Appl. Phys. **121**(2), 023108 (2017).
31. H. Ito, M. Ogawa, and S. Sunaga, "Evaluation of an organic light-emitting diode display for precise visual stimulation," J. Vis. **13**(7), 6 (2013).
32. Z. Ge, R. Lu, T. X. Wu, S.-T. Wu, C.-L. Lin, N.-C. Hsu, W.-Y. Li, and C.-K. Wei, "Extraordinarily wide-view circular polarizers for liquid crystal displays," Opt. Express **16**(5), 3120–3129 (2008).
33. K. Käläntär, "A directional backlight with narrow angular luminance distribution for widening the viewing angle for an LCD with a front-surface light-scattering film," J. Soc. Inf. Disp. **20**(3), 133–142 (2012).
34. Y. Gao, Z. Luo, R. Zhu, Q. Hong, S. T. Wu, M. C. Li, S. L. Lee, and W. C. Tsai, "A high performance LCD with wide luminance distribution," J. Disp. Technol. **11**(4), 315–324 (2015).
35. S. S. Kim, B. H. Berkeley, K. H. Kim, and J. K. Song, "New technologies for advanced LCD-TV performance," J. Soc. Inf. Disp. **12**(4), 353–359 (2004).
36. J. P. Yang, E. L. Hsiang, and H. M. Philip Chen, "Wide viewing angle TN LCD enhanced by printed quantum-dots film," SID Int. Symp. Digest Tech. Papers **47**(1), 21–24 (2016).
37. H. Chen, J. He, and S. T. Wu, "Recent advances on quantum-dot-enhanced liquid crystal displays," IEEE J. Sel. Top. Quantum Electron. **23**(5), 1900611 (2017).

1. Introduction

Virtual reality (VR) is an emerging wearable display which has widespread applications in immersive video games, sports training, and surgery simulation, just to name a few [1, 2]. Two critical requirements for VR displays are high resolution and fast response time. Unlike computers and TVs which are often placed more than 30 cm away from the viewers, the head-mounted VR display is near to the eye. Nowadays, most VR products, such as Oculus Rift and Samsung Gear VR, use organic light emitting diode (OLED) display panels because of their excellent black state, fast response time, and high resolution. For example, the resolution of Oculus Rift and Samsung Gear VR is about 461 and 577 pixels per inch (PPI) for each eye. However, VR displays require resolution density over 1000 PPI, which is not yet achieved by the current headsets using OLED displays. The resolution of OLED panel is limited by the employed mask and the relatively low aperture ratio because multiple thin-film transistors (TFTs) are required per pixel for current driving and compensation circuit. Therefore, liquid crystal displays (LCDs) which only need one switching TFT per pixel have

Optics EXPRESS

potential to achieve higher resolution for VR applications. For example, Sharp has developed an LCD prototype for VR headsets with 1008 PPI. However, traditional LCD modes, such as in-plane switching (IPS) and fringe field switching (FFS) suffer from slow response time, which results in motion blurs.

To speed up the response time, several approaches have been proposed, including polymer-stabilized blue phase LCs [3, 4] and uniform lying helix (ULH) LCs based on flexoelectro-optic effect [5–7]. Each technology has its own pros and cons. For example, blue phase LC offers submillisecond response time, but it requires protruded electrodes to achieve 75% transmittance at 15 V. On the other hand, ULH LC needs complicated molecular alignment process and its highest achievable contrast ratio so far is only ~300:1. For nematic devices, low viscosity LC together with an ultra-thin cell gap (d = 1.2 μm) could achieve submillisecond response time in a reflective liquid-crystal-on-silicon device [8]. On the device side, triode approach [9–11] enables fast rise time and decay time, but it requires two TFTs per pixel and the transmittance is compromised.

In this paper, we report a vertically-aligned cell with a negative dielectric anisotropy ($\Delta\varepsilon<0$) LC mixture, which is driven by the longitudinal field and the fringing field. The top substrate has a common electrode, while the bottom substrate consists of FFS structure, but with etched square-hole patterns on the pixel electrode. The average gray-to-gray (GTG) response time is 0.94 ms and peak transmittance is 85% at 7.5 V_{rms}. Besides, our device enables a high aperture ratio because only one TFT is needed per pixel while the bottom FFS electrodes have built-in capacitors. As a result, high resolution is achievable. This device is attractive for the emerging VR displays.

2. LC material

To achieve fast response time, low viscosity (γ_1) liquid crystal and thin cell gap (d) are favorable. However, there is a limit for squeezing the cell gap. The thinnest yet still manufacturable cell gap is about 2.5 μm. A thinner cell gap demands a higher birefringence (Δn) LC in order to obtain high transmittance, which in turn increases the rotational viscosity. Therefore, it is very important to balance all the LC properties during material design. To obtain high Δn while keeping a low visco-elastic constant (γ_1/K_{33}), we formulated a new nematic LC mixture designated as UCF-N6. It consists of 36 wt% ZOC-7003 (JNC, Japan) [12], 31 wt% SN0012N (Xi'an, China), 10 wt% HCCH 730700-200 (HCCH, China) and 23 wt% non-polar diluters. We measured the birefringence, dielectric anisotropy ($\Delta\varepsilon$), visco-elastic coefficient, and activation energy (E_a) of UCF-N6, and results are listed in Table 1.

Table 1. Measured physical properties of UCF-N6 at T = 25°C and f = 1 kHz.

	Δn @ λ = 550 nm	$\varepsilon_{//}$	$\varepsilon_{\perp}$	$\Delta\varepsilon$	γ_1 (mPas)	K_{33} (pN)	γ_1/K_{33} (ms/μm^2)	T_c (°C)	E_a (meV)
UCF-N6	0.1587	3.63	6.66	–3.03	105.1	17.5	6.01	80.2	247.7

2.1 Birefringence

To measure Δn at different temperatures, we first injected UCF-N6 into a commercial VA cell with cell gap $d \approx 9$ μm. Then the cell was placed on a Linkam heat stage controlled by TMS94 Temperature Programmer and sandwiched between two crossed polarizers. The probing light source was a He-Ne laser (λ = 632.8 nm). A 1 kHz square-wave AC voltage was applied to the LC cell. Birefringence at each temperature was obtained from the phase retardation $\delta = 2\pi d\Delta n/\lambda$ [13]. Results are plotted in Fig. 1, where dots are experimental data and solid line is theoretical fitting with Haller's semi-empirical equation [14]:

$$\Delta n(T) = \Delta n_0 S = \Delta n_0 (1 - T / T_c)^{\beta}. \quad (1)$$

Optics EXPRESS

In Eq. (1), Δn_0 is the extrapolated birefringence at $T = 0$ K, S is the order parameter, T_c is the clearing point of LC, and β is a material constant. Through fitting, we found $\Delta n_o = 0.213$ and $\beta = 0.194$ for UCF-N6.

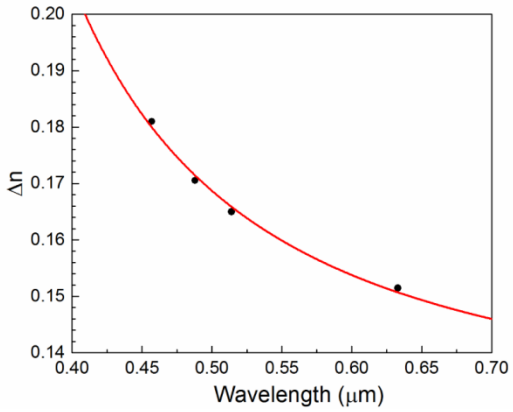

Fig. 1. Temperature dependent birefringence of UCF-N6 at λ = 633 nm. Dots are measured data and solid line is fitting curve with Eq. (1).

Next, we measured Δn at different wavelengths in order to investigate the electro-optic performance at RGB colors. The probing light sources are a tunable Argon ion laser (λ = 457 nm, 488 nm, and 514 nm) and a He-Ne laser. Figure 2 shows the measured results (dots) and fitting curve (solid line) with the single-band birefringence dispersion equation [15]:

$$\Delta n = G\frac{\lambda^2 \cdot \lambda^{*2}}{\lambda^2 - \lambda^{*2}}. \tag{2}$$

Here, G is a proportionality constant and λ^* is the mean resonance wavelength. The obtained fitting values are: $G = 2.124\ \mu m^{-2}$ and $\lambda^* = 0.246$ μm. From Eq. (2), we can calculate the birefringence at any wavelength. Results are $\Delta n = 0.181$ at λ = 450 nm, 0.159 at 550 nm, and 0.148 at 650 nm. These data will be used in the device simulation later.

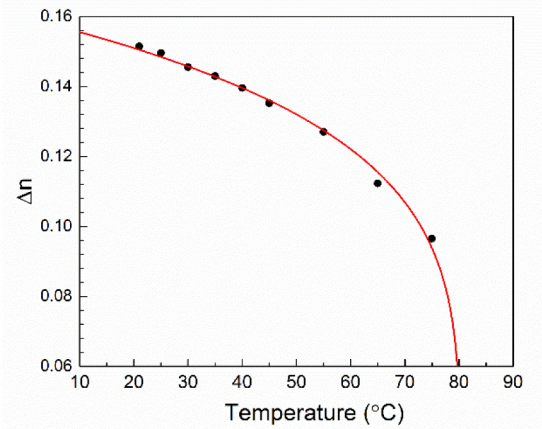

Fig. 2. Wavelength dependent birefringence of UCF-N6 at T = 25°C. Dots are measured data and solid line is fitting curve with Eq. (2).

Optics EXPRESS

2.2 Visco-elastic coefficient

LC response time is linearly proportional to γ_1/K_{33}, which is highly dependent on the temperature. From the transit relaxation time measurement, we can extract the γ_1/K_{33} value.

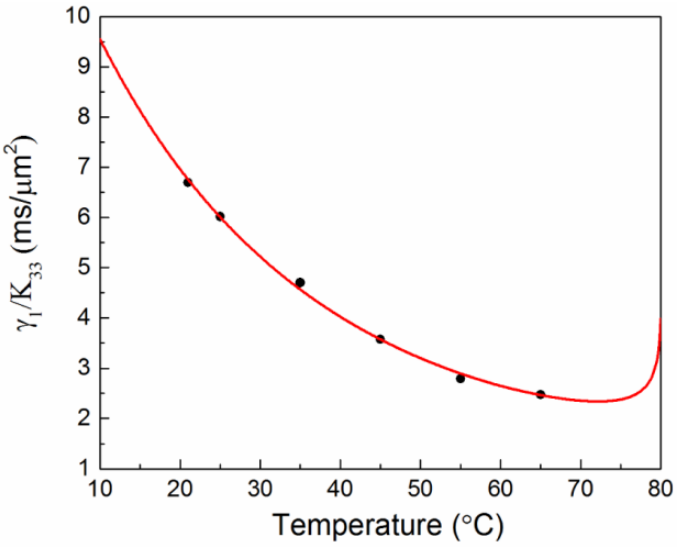

Fig. 3. Temperature dependent visco-elastic coefficient of UCF-N6. Dots are measured data and solid line is fitting curve with Eq. (3)

Figure 3 depicts the γ_1/K_{33} at different temperatures, in which dots represent experimental data. As the temperature increases, γ_1/K_{33} decreases exponentially. The solid line is fitting curve with following equation [16]:

$$\frac{\gamma_1}{K_{33}} = A \cdot \frac{\exp(E_a / k_B T)}{(1 - T / T_c)^{\beta}}, \tag{3}$$

where A is a proportionality constant, k_B is the Boltzmann constant, E_a is the activation energy, and β is the material constant obtained from Eq. (1). For an LC material, activation energy determines the decreasing rate of γ_1/K_{33} as temperature increases [17]. Through fitting, we found E_a = 247.7 meV. At T = 25°C, γ_1/K_{33} of UCF-N6 is 6.01 ms/μm^2, and the corresponding γ_1 is 105.1 mPas, and bend elastic constant K_{33} = 17.5 pN.

3. Device structure and simulation results

To achieve submillisecond response time, developing LC material with low γ_1/K_{33} alone is inadequate. On the device side, here we propose a new structure as Fig. 4 depicts. The top substrate has a 50-nm planar common electrode grounded at V = 0. The bottom substrate (Fig. 4(a)) consists of three layers: 50-nm transparent planar common electrode (V = 0), a 400-nm passivation layer, and 50-nm pixel electrode with square-shaped holes. Figure 4(b) shows the patterns and dimensions of the holes. The detailed sizes of g and w will be discussed later. The bottom electrode configuration is similar to the fringing field switching (FFS) [18], except for the patterned square holes and the LC with $\Delta\varepsilon<0$ is in vertical alignment (VA).

Optics EXPRESS

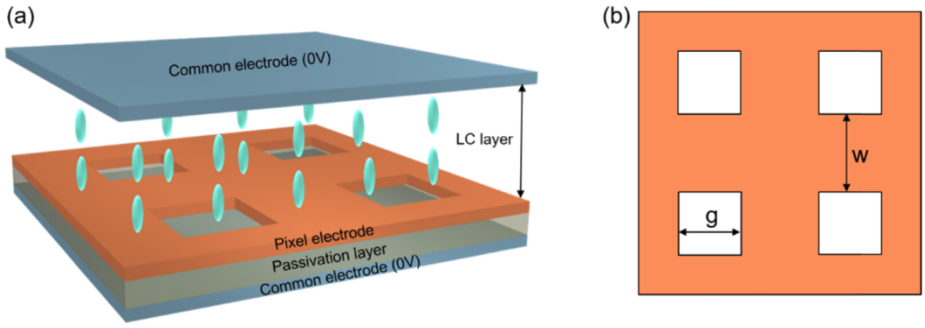

Fig. 4. (a) Device structure of the proposed VA⊕FFS cell, and (b) top view of the pixel electrode.

To achieve high transmittance and good dark state for wide-view purpose, the LC cell is sandwiched between two circular polarizers and a set of compensation films. When there is no voltage applied, all the LC directors are vertically aligned (pre-tilt angle = 0°), as Fig. 4(a) depicts. The light passing through the LC layer experiences no phase retardation and is blocked by the crossed circular polarizer, leading to an excellent dark state. As the voltage exceeds a threshold, the LC directors are reoriented by the vertical field outside the hole area and the fringing field surrounding the hole area. For convenience, let us call this hybrid operation mode as VA⊕FFS. Similar to patterned vertical alignment (PVA) mode [19], the oblique component of the fringing field prevents LC directors from reorienting randomly even though the pre-tile angle is 0°. Figures 5(a) and 5(b) depict the top view and cross-sectional view of LC director distributions, respectively, at a voltage-on state (7.5 V_{rms}). Because of symmetry, the LC directors at the center of the square holes and the pixel electrodes do not reorient (if the voltage is not too high), which function as standing walls to provide strong restoring force for improving decay time [20, 21]. On the down side, these vertical standing walls decrease the transmittance, thus, their dimensions should be optimized. Also through simulation, we found that the pixel electrode with square holes exhibits similar performance with circular holes and rounded-square holes, indicating that our VA⊕FFS mode enables a relatively large fabrication tolerance.

Optics EXPRESS

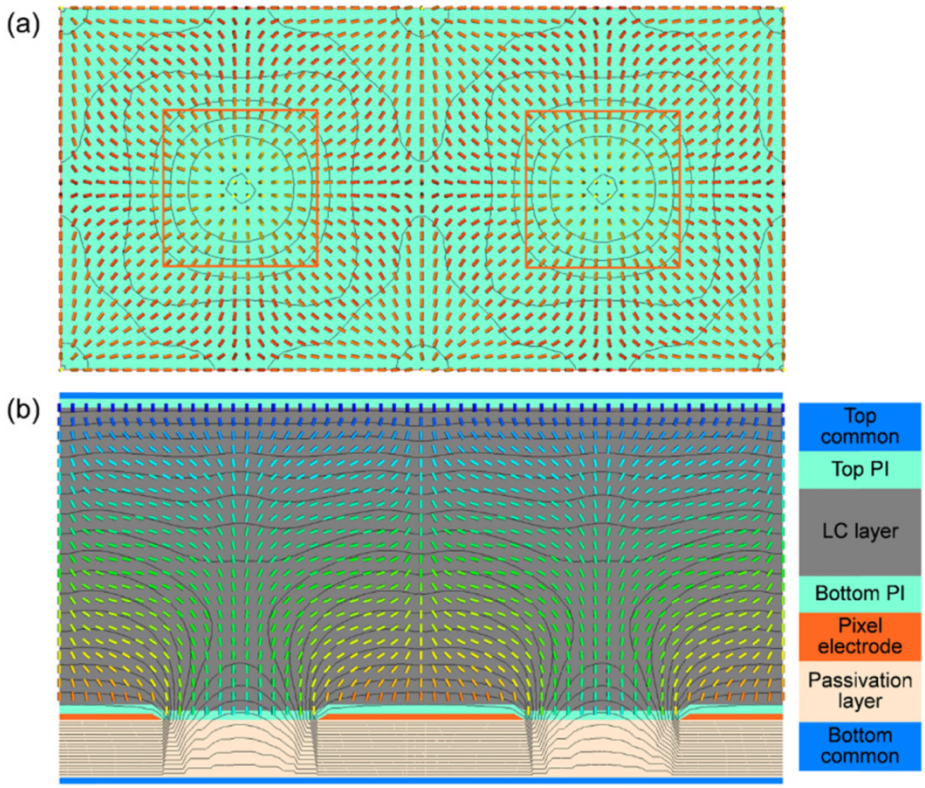

Fig. 5. (a) Top view and (b) cross-sectional view of simulated LC director distributions of the VA⊕FFS cell at 7.5 V_{rms}. PI = polyimide.

From Fig. 5, we can see that the LC directors inside the hole area are primarily affected by the symmetric fringing fields so that they are radially distributed. However, on top of pixel electrodes, the LC directors are influenced by both longitudinal and fringing fields. Because of these spatially nonuniform LC reorientations, crossed circular polarizers are preferred to achieve high transmittance. Figure 6 illustrate the top view of transmittance profiles with crossed linear polarizers and circular polarizers. For linear polarizers, the light transmitting though the first polarizer experiences no phase retardation if the LC directors distributed along the transmission axis of linear polarizer. As a result, the light will be blocked by the analyzer, leading to transmittance dead zone shown in Fig. 6(a). In the case of crossed circular polarizers (Fig. 6(b)), the circularly polarized light is independent of the LC director's orientation angle, thus a higher transmittance is achieved.

Optics EXPRESS

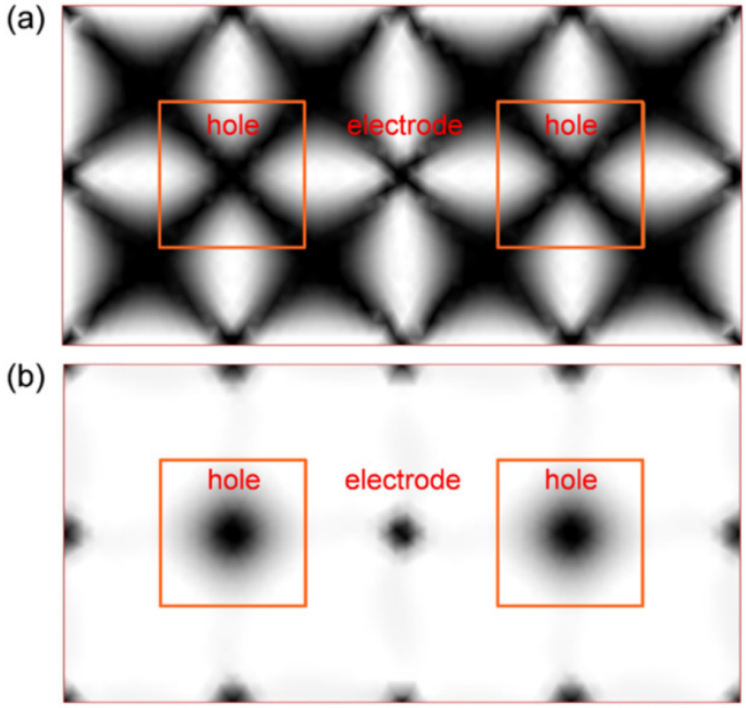

Fig. 6. Top view of on-state transmittance profiles of the VA⊕FFS cell with crossed (a) linear polarizers and (b) circular polarizers, at V_{on} = 7.5 V_{rms}.

3.1 Electrode structure optimization

To optimize the performance of our VA⊕FFS mode, we conducted device simulation with a commercial LC simulator TechWiz LCD 3D (Sanayi, Korea) and calculated the electro-optic properties by the extended 2 × 2 Jones matrix method [22]. The anchoring energy of the alignment layer is set to be strong. Figure 7 shows the simulated voltage-dependent transmittance (VT) curves for the VA⊕FFS structure with different electrode width (w) and electrode gap (g). The LC material is UCF-N6 with cell gap d = 2.6 μm, which is manageable with the current fabrication technology. To enhance transmittance, a circularly polarized light is employed because it is independent of the LC director's reorientation angle.

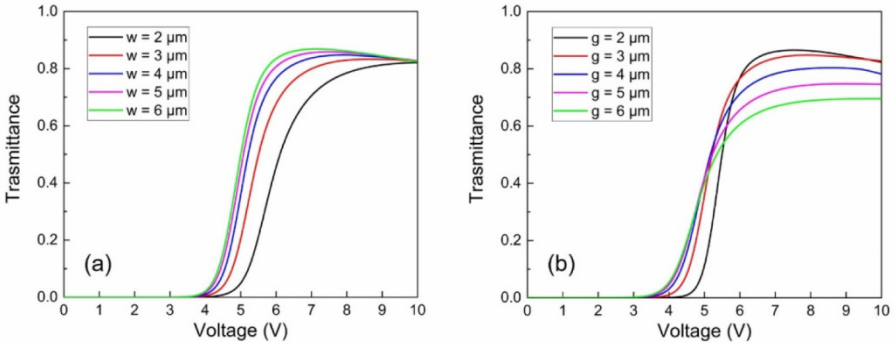

Fig. 7. Simulated VT curves for VA⊕FFS cells using UCF-N6: (a) keeping g = 3 μm and varying w from 2~6 μm, and (b) keeping w = 4 μm, and varying g from 2~6 μm.

Optics EXPRESS

As illustrated in Fig. 7(a), when we keep g = 3 μm and change the electrode width from 2 μm to 6 μm, the peak transmittance increases and V_{th} decreases. The reason is that as the electrode area become wider, the vertical electric field between top common electrode and bottom pixel electrode is dominant, which means that the VA⊕FFS cell behaves more like a VA cell. Therefore, high transmittance and low V_{th} are obtained. On the other hand, when we keep w = 4 μm and change g from 2 μm to 6 μm, both peak transmittance and V_{th} decrease (Fig. 7(b)). Because when g increases, more LC molecules at the center of the electrode gap do not reorient, resulting in a larger dead zone area.

Figure 8 shows the corresponding rise time and fall time of our VA⊕FFS cells. As the electrode width (Fig. 8(a)) and electrode gap (Fig. 8(b)) increase, the fall time gradually increases. As mentioned above, because the LC directors at the center of the pixel electrode and square-shaped holes do not reorient, they act as virtual walls to provide strong restoring force for reducing the response time. However, the distance between these virtual walls increases as the electrode width and electrode gap keep increasing. As a result, the restoring force exerted by the virtual walls become weaker, leading to slower fall time. In order to obtain high transmittance, low operation voltage and fast response time, we choose w = 4 μm and g = 3 μm for further calculation.

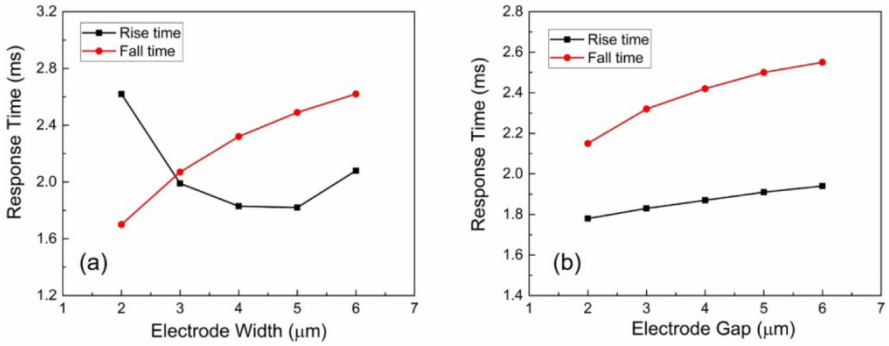

Fig. 8. Simulated response time for our VA⊕FFS cells using UCF-N6. (a) g = 3 μm and w = 2~6 μm, and (b) w = 4 μm and g = 2~6 μm.

Figure 9 depicts the simulated VT curves of our optimized VA⊕FFS cell at the specified red, green and blue colors. By using circular polarizers, the peak transmittance can reach 85% at 7.5 V_{rms} for λ = 550 nm, which is comparable to the 2-domain nFFS mode (~85%) [23].

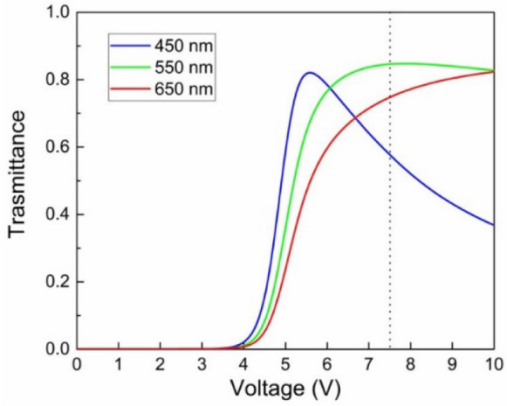

Fig. 9. Simulated VT curves of the proposed VA⊕FFS cell at the specified wavelengths. d = 2.6 μm, w = 4 μm, and g = 3 μm.

Optics EXPRESS

Another LC mode with submillisecond response time is vertically-aligned in-plane-switching (VA-IPS) with 2D electrodes [11, 24, 25]. Figure 10(a) illustrates the cross-sectional view of VA-IPS mode [11]. The bottom substrate consists of two electrodes: planar common electrode (V_{com}) and interdigital pixel electrodes (Electrodes 1 and 2) separated by a thin passivation layer. This structure utilizes both fringing fields between pixel electrodes and common electrode, and in-plane field between pixel electrodes [26]. Voltages with the same magnitude but reversed polarities are applied to Electrodes 1 and 2, respectively. Therefore, two TFTs per pixel is required. On the other hand, the top substrate has a planar counter electrode ($V_{counter}$) with a biased voltage, e.g. $V_{counter}$ = 5 V_{rms}. Therefore, both rise and decay processes are accelerated by the electric fields, which greatly improve the response time. In the simulation, we set the electrode width w = 2 μm, electrode gap l = 5 μm, and cell gap d = 4 μm. The LC material is TL-203 (Merck), and its physical properties are: Δn = 0.201 at λ = 550 nm, $\Delta\varepsilon$ = 11, K_{11} = 15.8 pN, K_{33} = 17.9 pN, and rotational viscosity γ_1 = 150 mPas. Figures 10(b) and 10(c) show the simulated VT curve and response time curve for the VA-IPS mode. The rise time is 1.53 ms at 9.3 V_{rms} and decay time 0.97 ms. Such a fast response time helps suppress image blurs. However, the tradeoffs are relatively high operation voltage and low transmittance. At 9.3 V_{rms}, the transmittance is only 63.3%. In order to boost transmittance, we can increase the electrode gap, but the voltage will also increase. Another method is to reduce $V_{counter}$, but the response time will be compromised.

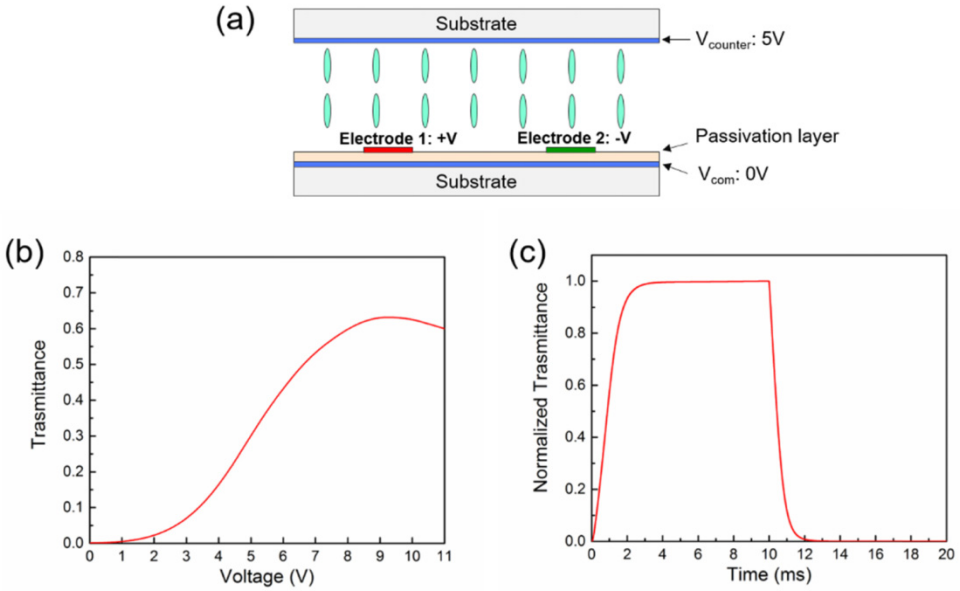

Fig. 10. (a) The cross-sectional structure, (b) the simulated VT curve at λ = 550 nm, and (c) the simulated time-dependent transmittance curve of a VA-IPS LCD at 9.3 V_{rms}.

Different from VA-IPS which employs a positive Δε LC, our VA⊕FFS uses a negative Δε LC. The transmittance of VA⊕FFS mode consists of two parts: vertical field-induced LC reorientations outside the hole area and fringe field-induced LC reorientations near the hole area. Besides, the fast decay time achieved in VA⊕FFS mode is not due to the vertical electric field, but the standing LC directors at the center of the hole and the pixel electrodes. These LC molecules function as virtual walls to provide strong restoring force for improving decay time.

Optics EXPRESS

3.2 Motion picture response time

To obtain the gray-to-gray (GTG) response time of our VA⊕FFS cell, we divided the VT curve at λ = 550 nm uniformly into eight gray levels and calculated the response time between different gray levels. The response time is defined as the time interval between 10% and 90% transmittance change. Results are summarized in Table 2. By applying overdrive and undershoot driving scheme [27], the average GTG response time is 0.94 ms. Such a fast response time helps to suppress the color breakup in a field sequential color display.

Table 2. Calculated GTG response time of the proposed VA⊕FFS cell. (unit: ms).

	1	2	3	4	5	6	7	8
1		0.75	0.88	1.00	1.12	1.27	1.47	1.83
2	1.53		0.27	0.48	0.66	0.86	1.10	1.53
3	1.63	0.45		0.21	0.41	0.61	0.87	1.35
4	1.72	0.75	0.31		0.20	0.41	0.68	1.23
5	1.83	0.98	0.57	0.26		0.22	0.50	1.14
6	1.95	1.21	0.81	0.51	0.25		0.30	1.09
7	2.11	1.44	1.06	0.77	0.52	0.27		1.11
8	2.32	1.72	1.37	1.10	0.86	0.64	0.40	

In a sample-and-hold type TFT LCD, motion image blur should be minimized. It is determined by the LC response time as well as TFT frame rate (f). To quantify the visual performance of a moving object on the screen, motion picture response time (MPRT) has been proposed [28, 29]. Recently, a simple yet accurate analytical equation relating MPRT with LC response time and frame rate has been derived [30]:

$$MPRT \approx \sqrt{\tau^2 + (0.8 \times T_f)^2}. \quad (4)$$

In Eq. (4), τ is the LC response time, T_f (= 1000/f) is the TFT frame time. Table 3 lists the calculated GTG MPRT at f = 144 Hz, which is the frame rate employed in commercial products such as game monitors. The average MPRT for the VA⊕FFS LCD is 5.66 ms.

Table 3. Calculated GTG MPRT of our VA⊕FFS LCD at f = 144 Hz. (unit: ms).

	1	2	3	4	5	6	7	8
1		5.61	5.62	5.64	5.67	5.70	5.75	5.85
2	5.76		5.56	5.58	5.59	5.62	5.66	5.76
3	5.79	5.57		5.56	5.57	5.59	5.62	5.72
4	5.82	5.61	5.56		5.56	5.57	5.60	5.69
5	5.85	5.64	5.58	5.56		5.56	5.58	5.67
6	5.89	5.69	5.61	5.58	5.56		5.56	5.66
7	5.94	5.74	5.66	5.61	5.58	5.56		5.67
8	6.02	5.82	5.72	5.66	5.62	5.59	5.57	

To mitigate image blur, MPRT should be about 1.5 ms, like CRT (cathode ray tube). But from Eq. (4), we know that even if LC response time is zero (τ = 0 ms), the MPRT is still as slow as 5.56 ms at f = 144 Hz. One way to reduce MPRT is to increase frame rate. Figure 11(a) shows MPRT versus LC response time at different frame rates. As frame rate increases, MPRT decreases almost linearly. When f = 480 Hz, the average MPRT is 1.97 ms, which is close to our targeted value. Moreover, for a high resolution LCD, e.g. 4K2K, operating at 480 Hz frame rate would demand a very short TFT charging time (1.08 μs). This is technically challenging by itself.

Optics EXPRESS

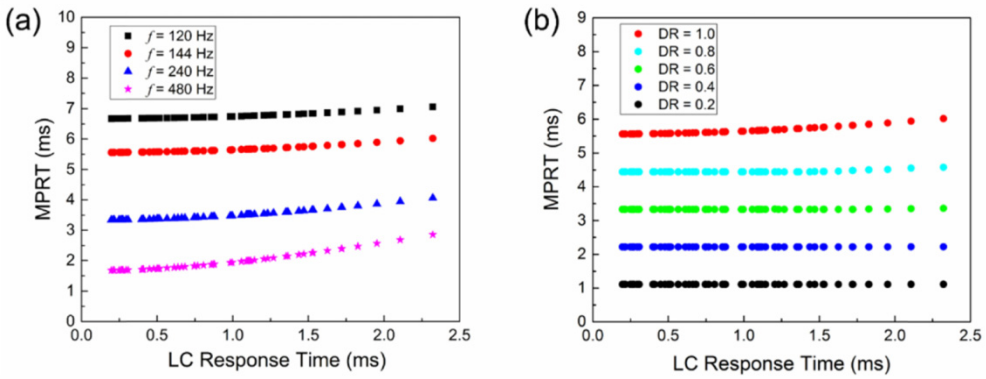

Fig. 11. MPRT as a function of LC response time (a) with different frame rates, and (b) with different duty ratio at f = 144 Hz.

A simpler method to reduce MPRT is through backlight modulation [31]. In the one frame time, the on-time ratio of the backlight is defined as duty ratio (DR). As illustrated in Fig. 11(b), when the LC response time is short, MPRT decreases linearly with the backlight duty ratio. For example, when DR = 0.2 at f = 144Hz, the average MPRT is only 1.11 ms, which is comparable to CRT. The reason is that the initial slow transition part of LC is obscured by the delayed backlight, which effectively suppresses the sample-and-hold effect. Such an operation mechanism is similar to impulse driving of CRT. Therefore, a low backlight duty ratio helps to minimize image blur, but the major tradeoff is decreased brightness. To remedy the decreased brightness, we could increase the driving current of the LED backlight or use a more efficient backlight.

For mobile displays, it is highly desirable to reduce the operation voltage to 5V. To do so, we could employ a LC material with higher Δε. The tradeoff is the increased viscosity, which in turn results in slower response time. However, even if the average GTG response time of our VA⊕FFS mode increases by 2X (≈2 ms), its MRPT (≈5.9 ms) is still relatively fast at f = 144 Hz. Besides, according to Fig. 11(b), at DR = 0.2 the MPRT stays constant even if the LC response time changes from 0 to 2.5 ms. Therefore, it is still feasible to use a LC material with higher Δε to reduce the driving voltage.

3.3 Viewing Angle and Gamma Shift

To widen the viewing angle of a LCD, compensation films are commonly employed. For example, for multi-domain vertical-alignment (MVA) LCDs, a biaxial film or a pair of positive A and positive C uniaxial films are often used. While for VA⊕FFS mode, we used circular polarizers instead of linear polarizers in order to obtain high transmittance. Therefore, compensation design for circular polarizers is required. In our simulation, we used the conventional Lambertian backlight and compensation scheme proposed by Ge, et al. [32]. First, a negative C-plate is used to partially compensate the phase retardation from the LC layer. After optimization, a biaxial plate is added to compensate the residual phase retardation from the negative C-plate and LC layer. The parameters of the negative C-plate and biaxial plate are as follows: $n_{e,C}$ = 1.5902, $n_{o,C}$ = 1.5866, $n_{x,B}$ = 1.5028, $n_{y,B}$ = 1.5000, $n_{z,B}$ = 1.5018, d_C = 47.7 μm, d_B = 74.0 μm. Figure 12 depicts the calculated isocontrast contour of our VA⊕FFS LCD with compensation films. The maximum contrast ratio is ~5065:1 and a contrast ratio over 100:1 is expanded to ~80° viewing cone.

Optics EXPRESS

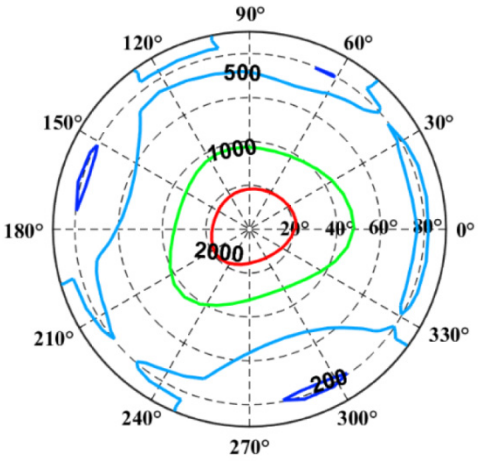

Fig. 12. Calculated isocontrast contour of VA⊕FFS LCD with compensation films.

To achieve a wider view angle, we could employ a directional backlight and a weak diffusive film [33, 34]. The directional backlight has a narrow angular luminance distribution: + 10°/-10° in the *x* direction (φ = 0~180°) and + 11°/-10° in the *y* direction (φ = 90~270°). The isocontrast contour (Fig. 13(a)) shows that the contrast ratio is improved to ~1000:1 over 60° viewing cone with the directional backlight and diffusive film combination.

In addition to view angle, gamma shift is another important concern for display devices. To quantitatively evaluate the off-axis image quality, an off-axis image distortion index (*D*) defined in [35] is used. When $D < 0.2$, the image distortion is indistinguishable by the human eye. With the directional backlight and diffusive film, we could achieve D = 0.171 (Fig. 13(b)). Besides, the diffusive film could be replaced by a quantum dot array to widen the viewing angle while keeping a wide color gamut [36, 37].

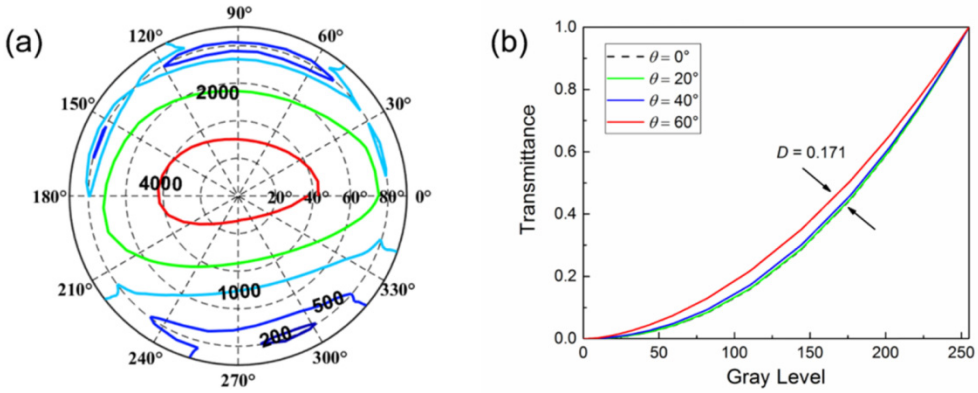

Fig. 13. Calculated (a) isocontrast contour and (b) gamma curves at view angle θ = 0°, 20°, 40°, 60° and φ = 0° with a directional backlight and compensation films.

4. Conclusion

We have proposed a three-dimensional pixel electrode design for vertical aligned fringe field switching LCDs. When filled with our newly developed LC mixture with $\Delta\varepsilon = -3.03$ and low visco-elastic coefficient (γ_1/K_{33} = 6.01 ms/μm^2 @ 25°C), we can achieve submillisecond response time. By increasing the driving frequency to 144 Hz and decreasing the duty ratio to 20%, we obtained MPRT ≈1.1 ms, which is comparable to CRT. Moreover, the peak

Optics EXPRESS

transmittance can reach 85% at 7.5 V_{rms} using crossed circular polarizers. Potential application of our VA⊕FFS for the wearable VR displays is foreseeable.

Funding

a.u.Vista, Inc.

Acknowledgments

The authors would like to thank Fenglin Peng for helpful discussion, Minggang Hu for providing mixture SN0012N, and a.u.Vista, Inc. for financial support.

132.170.208.112 {ts '2017-03-26 16:59:01'}